G3, 2021, 11(8), jkab169
DOI: 10.1093/g3journal/jkab169
Advance Access Publication Date: 14 May 2021
Investigation

DNA templates with blocked long 3′ end single-stranded overhangs (BL3SSO) promote bona fide Cas9-stimulated homology-directed repair of long transgenes into endogenous gene loci

Saptaparni Bandyopadhyay,[1,†] Joseph Douglass,[1,†] Sebastian Kapell,[1,2] Nazimuddin Khan,[1,2] Fabiana Feitosa-Suntheimer,[2] Jenny A. Klein,[3,4] Jasmine Temple,[3] Jayce Brown-Culbertson,[1] Alexander H. Tavares,[1,2] Mohsan Saeed,[1,2,*] and Nelson C. Lau[1,2,5,*]

[1]Department of Biochemistry, Boston University School of Medicine, Boston University, Boston, MA 02118, USA
[2]National Emerging Infectious Diseases Laboratories (NEIDL), Boston University, Boston, MA 02118, USA
[3]Department of Biology, Brandeis University, Waltham, MA 02453, USA
[4]Department of Anatomy and Neurobiology, Boston University School of Medicine, Boston University, Boston, MA 02118, USA
[5]Genome Science Institute, Boston University School of Medicine, Boston University, Boston, MA 02118, USA

*Corresponding author: Email: msaeed1@bu.edu (M.S.); nclau@bu.edu (N.C.L.)
[†]These authors contributed equally to this work.

Abstract

Knock-in of large transgenes by Cas9-mediated homology-directed repair (HDR) is an extremely inefficient process. Although the use of single-stranded oligonucleotides (ssODN) as an HDR donor has improved the integration of smaller transgenes, they do not support efficient insertion of large DNA sequences. In an effort to gain insights into the mechanism(s) governing the HDR-mediated integration of larger transgenes and to improve the technology, we conducted knock-in experiments targeting the human *EMX1* locus and applied rigorous genomic PCR analyses in the human HEK293 cell line. This exercise revealed an unexpected molecular complication arising from the transgene HDR being initiated at the single homology arm and the subsequent genomic integration of plasmid backbone sequences. To pivot around this problem, we devised a novel PCR-constructed template containing blocked long 3′ single-stranded overhangs (BL3SSO) that greatly improved the efficiency of bona fide Cas9-stimulated HDR at the *EMX1* locus. We further refined BL3SSO technology and successfully used it to insert GFP transgenes into two important interferon-stimulated genes (ISGs) loci, *Viperin/RSAD2*, and *ISG15*. This study demonstrates the utility of the BL3SSO platform for inserting long DNA sequences into both constitutive and inducible endogenous loci to generate novel human cell lines for the study of important biological processes.

Keywords: Cas9; HDR; gene tagging; BL3SSO; interferon-stimulated genes

Introduction

Genome editing by the programmed *Streptococcus pyogenes* Cas9 endonuclease (hereafter referred to as Cas9) in animal cells mainly triggers nonhomologous end joining (NHEJ) events that introduce insertions and deletions after DNA repair (Jasin and Haber 2016; Komor *et al.* 2017). Supplying short single-stranded oligonucleotides (ssODNs) with homology to the Cas9-cleaved site triggers relatively efficient homology-directed repair (HDR), which can be used to insert short heterologous DNA sequences into the genome (Lee *et al.* 1998; Chen *et al.* 2011; Hwang *et al.* 2013a, 2013b; Ran *et al.* 2013a; Kim *et al.* 2014; Paquet *et al.* 2016; Richardson *et al.* 2016). With ssODNs, other studies have proposed that the mechanism by single-stranded template repair via the Fanconi anemia pathway may likely resolve HDR (Davis and Maizels 2014; Jasin and Haber 2016; Richardson *et al.* 2018). However, although ssODNs work well for small modifications, chemical synthesis of such templates containing larger transgenes is technically challenging. Similarly, enzymatic methods to generate over 500 nt long single-stranded DNAs (lssDNAs) (Quadros *et al.* 2017; Codner *et al.* 2018) are complicated and expensive. An alternative is the use of double-stranded DNA (dsDNA) templates, such as plasmids or PCR-amplified DNA fragments, that can harbor large transgene sequences (Mali *et al.* 2013; Bottcher *et al.* 2014; Byrne *et al.* 2015; Chu *et al.* 2015; Gutschner *et al.* 2016; Codner *et al.* 2018). The use of dsDNA templates, however, has its own challenges and shortcomings. For example, blunt ends of PCR-amplified templates trigger DNA damage signaling, whereas plasmids display very low efficiency of seamless HDR (Hemmi *et al.* 2000; Ishii *et al.* 2006; MacDougall *et al.* 2007; Shiotani and Zou 2009).

Since ssODNs have a limited utility for insertion of large transgenes, some previous studies have explored the use of lssDNAs

Received: February 15, 2021. **Accepted:** May 03, 2021

that can be generated either by reverse-transcription of an *in vitro* transcribed RNA of the repair template (Quadros *et al.* 2017; Codner *et al.* 2018; Miura *et al.* 2018) or via asymmetric PCR followed by selective precipitation to enrich for a single DNA strand (Fu *et al.* 2018; Veneziano *et al.* 2018; Minev *et al.* 2019). However, lssDNA methodologies have two limitations: (1) the product yields are low due to the linear amplification afforded by asymmetric PCR, and (2) lower fidelity of reverse transcriptase results in mutations in the template (Menendez-Arias *et al.* 2017).

To facilitate scalable and facile generation of repair templates for routine HDR, we initially focused on the use of bacterial plasmids because they are easy to generate and modify. We then explored several modifications of the plasmid-based platforms such as tethering the repair plasmid onto the Cas9 enzyme and conversion of plasmids into lssDNAs. To delve deeper into molecular mechanisms underlying Cas9-mediated HDR and to examine the efficiency of seamless DNA integration (Quadros *et al.* 2017; Aird *et al.* 2018; Savic *et al.* 2018; Yao *et al.* 2018; Minev *et al.* 2019; Gu *et al.* 2020), we performed systematic and thorough investigation of HDR-driven insertion of various large-size transgenes.

First, we re-examined issues with genomic PCR approaches routinely used to validate the integration of larger transgenes. Because most of these approaches use primers that span only the integration sites and not the whole transgene, they can engender misleading claims of bona fide transgene integration (Cong *et al.* 2013; Ran *et al.* 2013a, 2013b; Byrne *et al.* 2015). This workaround and the omission of a transgene-spanning genomic PCR has been argued previously as evidence of bona fide HDR, while dismissing the lower efficiency of DNA polymerases to amplify large (>4 kb) amplicons directly from genomic DNA. This claim of bona fide Cas9-stimulated HDR with plasmid templates has recently been unmasked by some studies where Southern Blotting was used to validate transgene integration at the *S100a8* locus in mouse and the *lnx2a* locus in zebrafish (Won and Dawid 2017; Skryabin *et al.* 2020).

The HEK293 cell line is the first and most commonly used mammalian cell line to study genome editing by Cas9 (Cong *et al.* 2013; Mali *et al.* 2013; Ran *et al.* 2013a) and continues to be a useful vessel for the development and validation of new genome editing technologies. However, despite the well-established ease of knocking out endogenous genes and knocking in small DNA sequences in these cells, the insertion of longer transgenes remains challenging (Ran *et al.* 2013a; Lin *et al.* 2014; Byrne *et al.* 2015; Chu *et al.* 2015; Maruyama *et al.* 2015; Gutschner *et al.* 2016; He *et al.* 2016a) and has not yet approached the robust efficiencies observed with ssODNs (Chen *et al.* 2011; Hwang *et al.* 2013a, 2013b; Ran *et al.* 2013a; Kim *et al.* 2014; Paquet *et al.* 2016). Other studies have also highlighted the low efficiency of HDR for large-size insertions. For example, a recent study used digital droplet PCR and FACS to examine the efficiency of bona fide HDR in HEK293T and other human cells and estimated it to be <1% (He *et al.* 2016b; Miyaoka *et al.* 2016), reflecting a common practice of needing to screen hundreds of single-cell clones to find a bona fide HDR integrant (Rouet *et al.* 1994; Jasin and Haber 2016). Our observation of lower HDR events in HEK293T cells are in accordance with the need to enrich for edited cells by puromycin selection and cell sorting.

In an effort to improve integration of a long transgene into the model human genomic locus of *EMX1* where Cas9-stimulated genome editing was originally described (Cong *et al.* 2013; Ran *et al.* 2013a, 2013b), we optimized transgene-spanning genomic PCR approaches to confirm bona fide HDR integration events. Our results resolve and explain the illusion of bona fide transgene integration with plasmid templates, while confirming that our novel DNA template with blocked long 3' single-stranded overhangs (BL3SSO, pronounced "blasso") can promote authentic HDR at endogenous loci like *EMX1*. Lastly, we demonstrate the utility of BL3SSO templates in bona fide Cas9-stimulated HDR by inserting green fluorescent protein (GFP) into two important interferon-stimulated genes (ISGs) loci (*Viperin/RSAD2*, and *ISG15*), creating HEK293 cell lines that serve as sensors of Type-I interferon and antiviral responses.

ISG15 is among the first set of ISGs induced immediately after virus infection, often in an interferon-independent and IRF3-dependent manner (Perng and Lenschow 2018), while *Viperin* is induced late during infection, mainly following production and subsequent binding of interferons to their receptors (Fitzgerald 2011; Lindqvist and Overby 2018; Ebrahimi *et al.* 2020). Importantly, *Viperin* is also upregulated in response to endotoxins, bacterial infections, and even immune stimuli, such as atherosclerotic lesions. Considering the importance of these and other ISGs in a wide spectrum of human diseases, there is increasing interest in understanding the molecular details of how ISG expression is regulated and what is their mechanism(s) of action. Research in this area has so far mainly relied on the use of reporter genes, such as luciferase or a fluorescent protein, cloned under an interferon-stimulated response element (ISRE) or *IFN-ß* promoter, and ectopically expressed in cells of interest (Pine *et al.* 1990; Patel *et al.* 2012; Gage *et al.* 2016; Vasou *et al.* 2018; Csumita *et al.* 2020). These reporters, however, have a limited ability to reveal the genetic and epigenetic regulation of ISG expression. The technology described in this study will allow fast and facile creation of cell lines carrying ISGs fused with different reporter genes, which will serve as a valuable tool to delineate the complexities of interferon signaling pathways.

Materials and methods

Cas9 and sgRNA expression plasmids and Cas9 western blot

The original Cas9 and sgRNA expression plasmids for human cells were purchased from Addgene (pJDS246_CMV_hCas9, #43861; pMLM3636_U6 sgRNA, #43860). We used PCR and cloning to fuse the SNAPf enzyme from New England Biolabs (NEB) with the C-terminus of Cas9. PCR was used to generate templates for expression of sgRNAs targeting *EMX1* (Cong *et al.* 2013; Ran *et al.* 2013a). The FE-format sgRNAs contained a modification that reduced premature transcription termination by RNA Pol III (Chen *et al.* 2013). The Western blot to detect Cas9 and Cas9-SNAP was performed using a 1:500 dilution of the anti-Cas9 monoclonal antibody [7A9] (EpiGentek), raised against the recombinant N-terminal fragment of *S. pyogenes* Cas9.

Plasmid transfection methods, sgRNA production, and Cas9 ribonucleoprotein transfections

HEK293FT and HeLa cells were a kind gift from the Robert Kingston lab, and were cultured under standard 37°C, 5% CO_2 conditions with DMEM and 10% FBS. Cells were cultured to 70% confluence in 6-well plates and then transfected with Lipofectamine LTX or Lipofectamine 3000 according to the Manufacturer's guidelines. Two days after transfection, fresh media containing 4 µg/ml puromycin was added to initiate cell selection, and the drug-selecting media was refreshed every 3 days. After the 6th day of selection, when most cells lacking stable transgene integration began to die, the puromycin concentration

was reduced to 0.5 μg/ml, and the cells were cultured for another 8 days. Selected cells were then split 1:2 to an additional 6-well plate so that one plate could be fixed with crystal violet for visual quantitation, while the other plate provided cells for genomic DNA extraction.

Plasmid-based transfections used a mix of 0.5 μg of plasmids expressing Cas9-original or Cas9-SNAP, 0.5 μg of plasmids expressing the sgRNA (sgRNA_20, 21, or 22), 0.05 μg of pMAXGFP to visualize the transfection efficiency, and 0.25–1 μg of pCNEPm3 Repair Template plasmid either in the intact form or nicked and subsequently labeled with benyzlguanine (BG1- or BG2-) or fluorescein (FL-) coupled oligo (see below).

sgRNAs were generated by *in vitro* transcription of oligonucleotide templates using EnGEN® sgRNA Synthesis kit (NEB). For each well of a 6-well plate, 2 μg of sgRNA was incubated with 40 pmoles of Cas9 NLS (20 μM Stock from NEB) protein in 10 μl of OptiMEM media (no serum) for 10 minutes at room temperature. The pCNEPm3 plasmids was then added at 1 μg (~0.23pmoles) with 70 μl of OptiMEM, 10 ng of pMAXGFP tracer plasmid, and 3 μl of P3000 Enhancer Reagent (Invitrogen). In another tube of 100 μl OptiMEM, the 3 μl of Lipofectamine 3000 Reagent (Invitrogen) was diluted and then mixed with the Cas9 RNPs for additional 10 minutes incubation at room temperature before finally adding to cells.

Generating BG-labeled plasmids, minicircles, lssDNAs, and long 3' single-stranded overhang fragments

The left and right homology arms of ~1.0 kb and ~0.7 kb, respectively, complementary to the *EMX1* locus were amplified from HEK293FT genomic DNA using oligos listed in Supplementary Table S1, and cloned into pCNEP to flank a PGK-promoter-driven puromycin acetyl-transferase resistance marker cassette. An array of Nt.BbvCI sites were then cloned into the pCNEP backbone to make pCNEPm3. The RNT1 and RNT2 oligos have the same sequence as the array of Nt.BbvCI sites in pCNEPm3, and are coupled to benzylguanine (BG) or fluorescein (FL) via incubation with the NHS-ester precursors.

To label pCNEPm3 plasmid with BG-RNT1/2 oligos, 30 μg of plasmid was nicked overnight at 37°C with Nt.BbvCI in CutSmart buffer (NEB) followed by enzyme inactivation with 200 mM Tris-HCl and 400 mM EDTA, pH 8.0. A 400 μl reaction containing 25X molar excess of BG-RNT1/2 oligo was added and exchanged against the Nt.BbvCI nicked fragments from the plasmid by first heating to 85°C for 10 minutes and then cooling by 1°C per minute to 20°C. The labeled plasmid was precipitated with 3XPEGNaCl solution (30% w/v of PEG-8K in 1.6 M NaCl) for >2 hours at 4°C 21,000 g's centrifugation, washed twice with 80% ethanol, and resuspended in 250 μl of water. A 300 μl T4 DNA Ligase reaction was incubated at 16°C overnight, and then treated for 1 hour at room temperature with 1 μl of λ exonuclease to clear away remaining nicked plasmids.

To create a plasmid vector, pCHEP1, that was subsequently used to generate minicircles of lssDNAs, the EMX1-targeting cassette was PCR amplified from pCNEPm3 with primers that added Nt.BbvCI sites on either side of the cassette and enabled cloning into a pMC.0 mini-circle plasmid system from System Biosciences. Similarly, to create a plasmid vector, pCHEP2, that was later used to generate minicircles of long 3' single-stranded overhang (L3SSO) DNAs, primers with opposing Nt.BbvCI sites flanking only 100 bp of homology to *EMX1* were used to amplify the PGK-PuroR cassette that was then ligated together with the HiFi Gibson Assembly Master mix (NEB), and then cloned into pMC-0.

To generate minicircles, pCHEP1 was transformed into ZYCY10P3S2T cells (System Biosciences), grown to OD600 of 6.0 in 200 ml Terrific broth, and then washed and transferred to 400 ml of 1X induction medium for additional overnight growth. Minicircle plasmids were then purified by a standard ion-exchange maxiprep method and further purified by ExoV nuclease treatment that removed the contaminating bacterial genomic DNA fragments.

To generate lssDNA from pCHEP1 and L3SSO DNA from pCHEP2, 300 μg of intact plasmids purified by the standard ion-exchange maxiprep method was digested in 500 μl reactions with 35 μl of Nt.BbvCI enzyme (NEB) overnight at 37°C. The DNA was then precipitated and denatured in 600 μl of 2X Formamide Buffer (95% Formamide, 20 mM EDTA, 0.025% SDS, and 0.05% each Bromophenol Blue and Xylene Cyanol) at 95°C for 25 minutes followed by quick transfer to ice. The denatured DNA was resolved on a preparative 1% Low Melt agarose gel in 0.5X TAE buffer with standard ethidium bromide staining. The fastest running bands corresponding to the lssDNAs or the L3SSO DNAs were cut out and digested with Beta-agarase (NEB) and then mixed with 6 volumes of Buffer QX1 plus 1/10 vol of 3 M NaOAc, pH 5.0. To this mixture, 150 μl of QIAEX-II beads were added and incubated overnight. QIAXEX-II beads were then washed with 500 μl of Buffer QX1, 1 ml of Buffer PB, and 2 ml of Buffer PE before eluting in 100 μl of Elution Buffer EB heated to 50°C for 20 minutes.

Crystal violet and Methylene blue staining and quantitation

Cells rinsed once with 1X PBS were fixed with 2 ml of 3.7% formaldehyde in 1X PBS for 10 minutes at room temperature. After two additional rinses with 1X PBS, cells were stained with 2 ml of 0.05% Crystal violet dye in 10% methanol for 10 minutes at room temperature. Residual stain was washed with water, and the plates were scanned at 300 dpi at 16-bit grayscale and quantified with ImageJ. Initial studies used 0.2% Methylene blue dye in 50% methanol before we switched to the better imaging contrast of Crystal violet.

Genomic DNA extraction and Surveyor assays

Cells were lysed for at least 1 hour at 55°C in 300 μl lysis buffer (10 mM Tris pH 8.0, 100 mM NaCl, 10 mM EDTA pH 8.0, and 0.5% SDS, 120 μg Proteinase K), followed by 2 μl of RNase A digestion at 37°C for 30 minutes. After adding 200 μl of 0.5 M NaCl, the aqueous suspension was extracted against one volume of phenol/chloroform, and then genomic DNA was precipitated with 1 μl glycogen and 2 volumes 100% ethanol. After a 70% ethanol wash, DNA pellets were resuspended in 30 μl ddH_2O.

The SURVEYOR Assay (IDT Inc.) was conducted with PCR amplicons generated from genomic DNA with the EMX1_surveyor primers (see Supplementary Table S1) using 63°C annealing temperature. The heteroduplexes generated by slow cooling from 95°C to 25°C at 0.3°C/seconds were digested with Surveyor Nuclease and Enhancer S solutions for 30 minutes at 42°C before quenching with Stop solution and resolving on a 2% low-melt agarose gel stained with SYBR Gold (Invitrogen). Bands were imaged and quantified with ImageJ, following a calculation methodology described previously (Cong *et al.* 2013; Ran *et al.* 2013a).

Generation of BL3SSO PCR templates

Large scale PCRs generate the two pieces of targeting construct with opposing homology arms that will be converted into 3' SSO's while also blocking the 5' Biotin with Streptavidin. This protocol is partly inspired by a Zamore Lab protocol (Fu *et al.* 2018).

Step 1: Small-scale PCR to amplify Selection Marker (with or without promoter):

A 100 µl PCR reaction was set up using Biotin-coupled primers and a DNA template (from plasmid or PCR product). The cycling conditions comprised initial denaturation at 95°C for 2 minutes, followed by 25 cycles of 95°C, 30 seconds; 60–70°C, 30 seconds; and 72°C, 1–2 minutes, followed by an extension at 72°C for 2 minutes and hold at 20°C. Amplification was checked on 1% agarose gel and the amplicon sequence were confirmed by Sanger sequencing.

Step 2: Two separate large scale PCRs to add homology arms:

Two separate PCR mixes, each of 1.2 ml volume, were assembled using specific combinations of primers to put Biotin and IR-Dye-N on the 5' ends of opposite strands. Two microliters of PCR product from Step 1 was used as a template. 0.25 µM 5'Biotin oligo, 0.25 µM Outside Homology Arm oligo, and 0.02 µM Inside Homology Arm oligo (100mer that is the same sense as IR-Dye Oligo were added to the PCR reaction. The 1.2 ml reaction volume was then divided into 12 aliquots of 100 µl volume and subjected to 25 cycles of PCR. The PCR product from all 12 PCR tubes was then pooled back to obtain 1.2 ml volume. Fifty microliters of this reaction was saved for future diagnostic checks, for example, agarose gel electrophoresis and NanoDrop/Licor analysis for Before Beads/Denaturation Step. We obtained ~20 µg of DNA from each 1.2 ml PCR reaction, which translates into approximately 50 pmoles of DNA for a 1.5 kb amplicon.

Step 3: Binding of biotinylated DNA to NEB Streptavidin Mag Beads:

NEB Streptavidin Magnetic Beads (#S1420S) were completely resuspended into its storage buffer, and 0.5 mg beads (625 µl suspension) were dispensed into 1.5 ml tube for binding to a magnet. Beads were washed 2X in 1 ml of Wash Buffer [WB: 0.5 M NaCl, 20 mM Tris-HCl (pH 7.5), 1 mM EDTA]. Two ml of fresh Binding Buffer [BB: 2 M NaCl, 20% PEG 20 mM Tris-HCl (pH 7.5), 1 mM EDTA] was made (0.4 g of PEG8K powder was dissolved in fresh 2 ml of the salt solution), 1.6 ml BB was used to resuspended beads, and 800 µl of this BB mixture was split into four tubes with 200 µl each. The 1.2 ml Larger Scale PCRs (300 µl per tube) were added to the separate tubes of Streptavidin Mag Beads. The reaction was incubated at room temperature for 1 hour with gentle rotation. The solution was bound to magnet for 3 minutes. PCR supernatant was removed and collected in a new tube for later gel analysis. Beads were washed thoroughly 2X with 500 µl of WB, letting beads bind for 2 minutes.

Step 4: Denaturation of top strand lssDNA from bound Biotin-lssDNAs:

Three hundred microliters of 0.1 N NaOH was added to magnetic beads and incubated at room temp for 10 minutes. The mixture was left to bind to magnet for 3 minutes and the supernatant was collected in a new tube to analyze the depletion of biotinylated IssDNA molecules. NEB Mag beads were resuspended in 200 µl of 10 mM EDTA (pH 8.2).

Step 5: Release of biotinylated-lssDNAs from beads:

Mag Beads with biotinylated-lssDNAs were incubated at 70°C for 20 minutes and bound to magnet for 3 minutes. The eluate containing the biotinylated IssDNA was transferred to new tubes.

Step 6: Annealing of two eluted biotinylated-lssDNAs to form 3'SSOs:

Both eluted biotinylated-lssDNAs were combined into a new tube and mixed with 50 µl of 3 M NaCl and 50 µl of WBB followed by a 5 minutes incubation at 70°C. The solution was then cooled slowly to room temp for 10 minutes and subjected to another cycle of heating to 70°C for 5 minutes and cooling back to room temp for 10 minutes. Fifty microliters of this sample was saved for NanoDrop/Licor/Agarose Gel analysis with other samples to evaluate re-annealing and removal of non-biotin strand. One ml of 200proof Ethanol was added and incubated at −20°C for 1 hour to as long as overnight to precipitate and sterilize DNA for transfection. An input of Large Scale PCRs (~1.5 kb dsDNA bands), the Supernatant PCR after binding to Streptavidin Mag Beads (depletion of 1.5 kb dsDNA bands), NonBiotin-Denatured lssDNA strand from NaOH treatment (should run much faster than dsDNA band at ~half length), Eluted Biotin-lssDNA (should also run much faster than dsDNA band at ~half length), and Reannealed L3SSO (should be running back at ~1.5 kb dsDNA band) were run on 1% agarose gel.

Step 7: Pellet L3SSO DNAs and bind with Streptavidin to make BL3SSO:

The L3SSO DNA was pelleted down, washed with 70% ethanol, and resuspended in 100 µl of sterile 1X PBS (140 mM NaCl, 3.0 mM KCl, 4.0 mM Na2HPO4, 1.5 mM KH2PO4, pH 7.4) inside a biosafety cabinet. The concentration of the L3SSO was estimated with a Qubit reader. Greater than 12X molar excess of Streptavidin (NEB Streptavidin Solution, 1 mg/ml, N7021S, ~19 µM final concentration) was added to block 5' junction of L3SSO for 30 minutes on ice before transfecting this DNA into cells. For every transfection experiment, we prepared fresh BL3SSO and used it right away because its storage was found to drastically reduce the editing efficiency.

Genomic PCR assays

Primers for PCR-based analysis of the *EMX1* locus are listed in Supplementary Table S1. We assembled 50 µl PCR mix consisting of 200 ng of gDNA, 0.1 µM of each primer, 0.1 mM $MgCl_2$, 0.22 mM dNTPs, 1X Phusion GC-Buffer, 1.2 M Betaine, and 0.5 µl Phusion Polymerase (NEB). After an initial denaturation at 98°C for 2 minutes, the PCR mix was subjected to 30 cycles of 98°C, 1 minute; 63°C, 0.5 minute; and 72°C, 1.5–3.0 minutes depending on amplicon. For genomic PCR to detect the L3SSO integrant that would generate Amplicon-C', the primary (1°) PCR included 0.1 µM of the Poison primer with Outside primers to generate both the proper-HDR Amplicon-C' and a shorter Amplicon-F that competes against Amplicon-C_2. After 30 cycles, the 1° PCR product was diluted 1000-fold and used as a template in the secondary (2°) PCR with Inside-nested primers that would generate a ~0.6 kb Amplicon-C_2 from the Nonedited *EMX1* locus, and a ~1.5 kb Amplicon-C_2' with proper HDR of the L3SSO DNA. PCR to generate Amplicons-A and -B from cells transfected with L3SSO DNA worked best when we used 1X Phusion HF-buffer instead of the GC-buffer.

Primers for analyses of gene editing at Viperin/RSAD2 and *ISG15* loci are listed in Supplementary Table S1. Primary genomic

PCRs with poison primers and the subsequent secondary PCRs to characterize bona fide HDR in *Viperin* and *ISG15* cell clones were carried out similarly as for *EMX1* locus using transgene-spanning primers except that now poison primers were no longer required (Supplementary Table S1). The amplicons were cloned into pCR4-Blunt plasmid using the TOPO Cloning kit (Invitrogen) followed by plasmid propagation in bacteria. Bacterial colonies bearing correct-sized inserts were identified and the results were confirmed by Sanger sequencing.

IFN-α induction, analytical flow cytometry, FACS, and clonal analyses

One million HEK293FT cells were plated in each well of 6 well plates, transfected with Viperin/RSAD2- and ISG15- BL3SSO and Cas9 RNPs. Transfected cells were then grown for 48 hours before treating with either 1 nM IFN-α or 10 nM IFN-α for another 24 hours. Thereafter, the cells were subjected to either analytical flow cytometry or fluorescence activated cell sorting (FACS). Analytical flow cytometry was carried out on a LSR II instrument (BD Biosciences). Cells were washed with 1×PBS, centrifuged at 300 g for 5 minutes, fixed in 4% paraformaldehyde for 20 minutes, washed once again with 1×PBS and suspended in 1×PBS until analyzed.

FACS was performed on a FACSAria II (BD Biosciences) as per guidelines provided by Boston University Flow Cytometry Core Facility. Flow cytometry figure annotation, preparation and data analysis was done using the FlowJo software (FlowJo LLC). Cells were treated with 10 μM Calcein Blue (Invitrogen) for 15 minutes to stain live cells, washed with 1× PBS, trypsinized, pelleted at 300 g for 5 minutes, resuspended in 1 ml of 1XPBS + 1% BSA. The cells were recentrifuged and resuspended again in 3–6 ml of 1XPBS + 1% BSA and passed through disposable 5 ml polystyrene tubes with 40 μm strainer caps.

For selection of Viperin- and ISG15-Bl3ssoGFP clones, HEK293FT cells that were transfected with BL3SSO and Cas-9 RNP were treated with IFN-α and sorted through the FACSAria II as single cells into 96 well plates having conditioned media with Penicillin/Streptomycin and allowed to grow for 2–3 weeks undisturbed. Proliferating clones were transferred to 12- or 24- well plates, grown to 100% confluency and genomic DNA was extracted for genomic PCR. After positive clones are identified by genomic PCR and confirmed by western blot and GFP fluorescence imaging.

Fluorescence and Western blot analyses of GFP-tagged Viperin and ISG15 proteins

Cells were seeded into 6-well plates at a density of 1 million cells per well and treated with 1 and 10 nM concentrations of human IFN-α (PBL Assay Science) for 48 hours. For fluorescence, the cells were alive or fixed in 4% paraformaldehyde and imaged with an inverted Nikon epifluorescence microscope using 20X magnification, 100-ms exposure, and 1X gain. For Western blot, the cells were lysed in a RIPA buffer supplemented with 1X Roche cOmplete protease inhibitor cocktail. The protein concentration was measured by the BCA assay and normalized to 2 μg/μl. A total of 35 μg protein per lane was loaded on 4–12% tris-glycine precast gels and transferred to nitrocellulose membranes followed by detection of Viperin (Sigma; Cat. No. MABF106; 1:1000 dilution), ISG15 (Cell Signaling Technologies, RabMab # 2758S, 1:1000 dilution), beta-actin (Invitrogen, mouse monoclonal # 15G5A11/E2, 1:1000 dilution), and GFP (laboratory-made antibody; 1:4,000 dilution) antibodies.

Data availability

The data underlying this study are available in the article and in its online supplementary material. Supplementary material is available at figshare: https://doi.org/10.25387/g3.14442668.

Results and discussion

Establishing a system to couple Cas9 with a plasmid HDR template

Although other studies used a repair transgene to target HDR at a previously integrated fluorescent protein reporter transgene (Byrne *et al.* 2015; Chu *et al.* 2015; Maruyama *et al.* 2015; Gutschner *et al.* 2016; He *et al.* 2016a), we sought to examine the HDR conditions on *EMX1*, which can be considered a model endogenous gene that has been targeted by many previously described sgRNAs (Ran *et al.* 2013a, 2013b; Chen *et al.* 2017; Richardson *et al.* 2018) (Supplementary Table S1). We constructed an HDR template containing a PGK-promoter-driven puromycin resistance gene flanked on the right side by 0.7 kb and on the left side by 1.0 kb long homology arms targeting the human *EMX1* locus (Figure 1A) (Cong *et al.* 2013; Ran *et al.* 2013a). We also hypothesized that tethering the repair plasmid to the Cas9 enzyme might improve Cas9-stimulated HDR by increasing proximity and availability of all necessary elements. This notion has recently been applied to ssODN repair templates (Gu *et al.* 2018; Savic *et al.* 2018). In our study, we first fused Cas9 with the SNAP tag and then coupled this complex to the repair plasmid bearing a BG moiety. SNAP is an engineered variant of the human repair protein O^6-alkylguanine-DNA alkyltransferase (hAGT) that covalently reacts with the BG group (Juillerat *et al.* 2003; Gautier *et al.* 2008).

To test that C-terminal tagging of Cas9 with SNAP did not compromise the stability and genome editing capacity of the Cas9 enzyme, we evaluated the expression and activity of this fusion protein in HEK293FT cells (Juillerat *et al.* 2003). The steady-state expression level of Cas9-SNAP was appreciably lower than the unmodified enzyme (Figure 1B). However, surprisingly, the editing efficiency of the Cas9-SNAP fusion protein was higher than that of the wild-type enzyme, as demonstrated by increased DNA disruptions seen at the *EMX1* locus (Figure 1C). This suggests that fusion with SNAP may increase the turnover rate of Cas9, but it improves the editing efficiency of the enzyme, perhaps due to inherent DNA-binding potential of the SNAP protein (Juillerat *et al.* 2003).

We transfected HEK293FT cells with plasmids expressing Cas9, single guide RNA (sgRNA), and the repair template, and subjected them to puromycin selection for two weeks (Figure 1D). The logic behind this long selection was to obtain higher numbers of positive cells for rigorous analysis of the efficiency and accuracy of Cas9-stimulated HDR, which a recent study suggests is <1.0% in HEK293 cells (Miyaoka *et al.* 2016). The design of the *EMX1* transgene required that it is inserted in the chromosome in the same "direct" orientation as the endogenous gene, because no puromycin-resistant clones were recovered when the transgene was inserted in the "reversed" orientation (Figure 1, E and F). Additional details of how the transgene directionality influenced its expression have been provided in the Supplemental Text, Supplementary Figures S1 and S2.

Tethering the plasmid HDR template onto Cas9-SNAP does not enhance bona fide HDR

Previous studies on Cas9-stimulated HDR have mainly relied on amplification and analyses of the left and right junctions of the

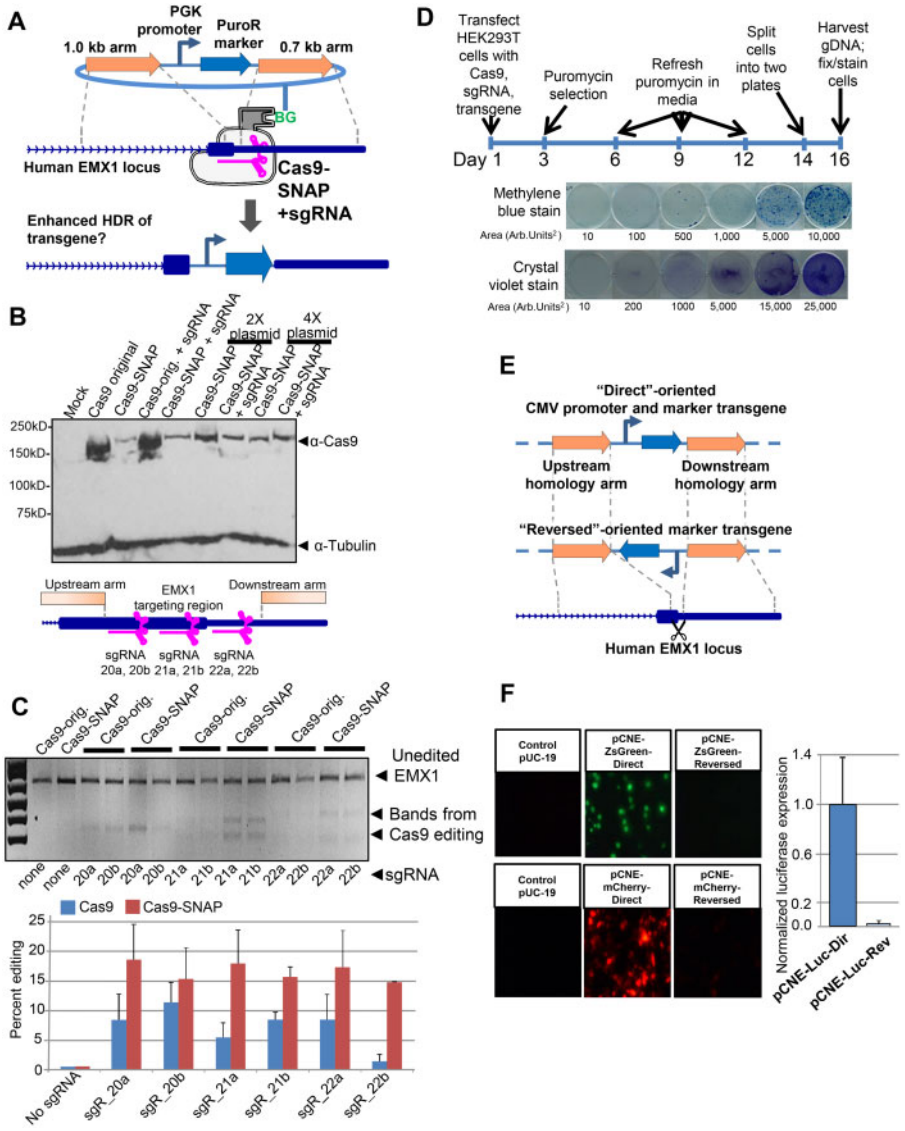

Figure 1 Establishing a Cas9-SNAP enzyme and plasmid transgene tethering system. (A) Concept to tether a plasmid with a BG-moiety to a Cas9-SNAP enzyme, where the DNA is template for HDR to the *EMX1* locus. (B) Western blot showing reduced steady-state levels of Cas9-SNAP compared to the original Cas9 expressed in HEK293FT cells. The graphic in the bottom panel shows the location of the three sgRNAs previously shown to effectively target the *EMX1* locus with "a" and "b" representing biological replicates. (C) Top panel is a representative gel of a SURVEYOR assay confirming the cutting and editing capacity of *EMX1*-targeting sgRNAs. The graph at the bottom shows increased editing capacity of Cas9-SNAP compared to the original Cas9. Error bars report the standard deviation from three technical replicates. (D) Selection strategy for puromycin-resistant cells and staining methodology to quantitate selected cells. (E) Illustration of the "Direct" (Dir) *vs* "Reversed" (Rev) transgene orientation with respect to the *EMX1* gene. (F) Effect of the "Direct" vs "Reversed" orientation on the transgene expression. The left panel shows the expression of the ZsGreen and mCherry transgenes, whereas the right panel shows the expression of the luciferase transgene.

integrated transgene (Ran *et al.* 2013a; Lin *et al.* 2014; Byrne *et al.* 2015; Chu *et al.* 2015; Maruyama *et al.* 2015; Gutschner *et al.* 2016; He *et al.* 2016a), leading to wide-ranging estimates of <1 to ~30% HDR efficiency. We hypothesized that the successful amplification of the junction sequences is not an accurate measure of bona fide HDR and therefore decided to apply a multipronged strategy to amplify both the junction sites and the whole transgene, to gain high-confidence estimates of the HDR efficiency. For this, we first optimized conditions to amplify *EMX1* sequences surrounding the transgene integration site specified by the targeting sgRNAs (Figure 2A, Amplicon-C in Figure 2B). The amplicons generated from the left transgene junction are designated as Amplicon-A, from the right junction as Amplicon-B, and from the whole transgene, including the junction sites, as Amplicon-C'.

We also first made sure that primers pairing to the region flanking the HDR cassette could directly amplify up to a 3.6 kb amplicon (Amplicon-E) from the unedited *EMX1* locus in a single genomic PCR assay. This control experiment was necessary to rule out the possibility that the PCR assay could miss detecting a bona fide transgene inserted into the *EMX1* locus due to possible unforeseen genomic DNA issues in the locus that could prevent the generation of the 3.3 kb product Amplicon-C'. In summary, we set up this assay to be more stringent than other studies which have skipped the transgene spanning genomic PCR test (Ran *et al.* 2013a; Lin *et al.* 2014; Byrne *et al.* 2015; Chu *et al.* 2015; Maruyama *et al.* 2015; Gutschner *et al.* 2016; He *et al.* 2016a).

We transfected HEK293FT cells with the Cas9-SNAP plasmid along with either BG-labeled HDR plasmid or, as a

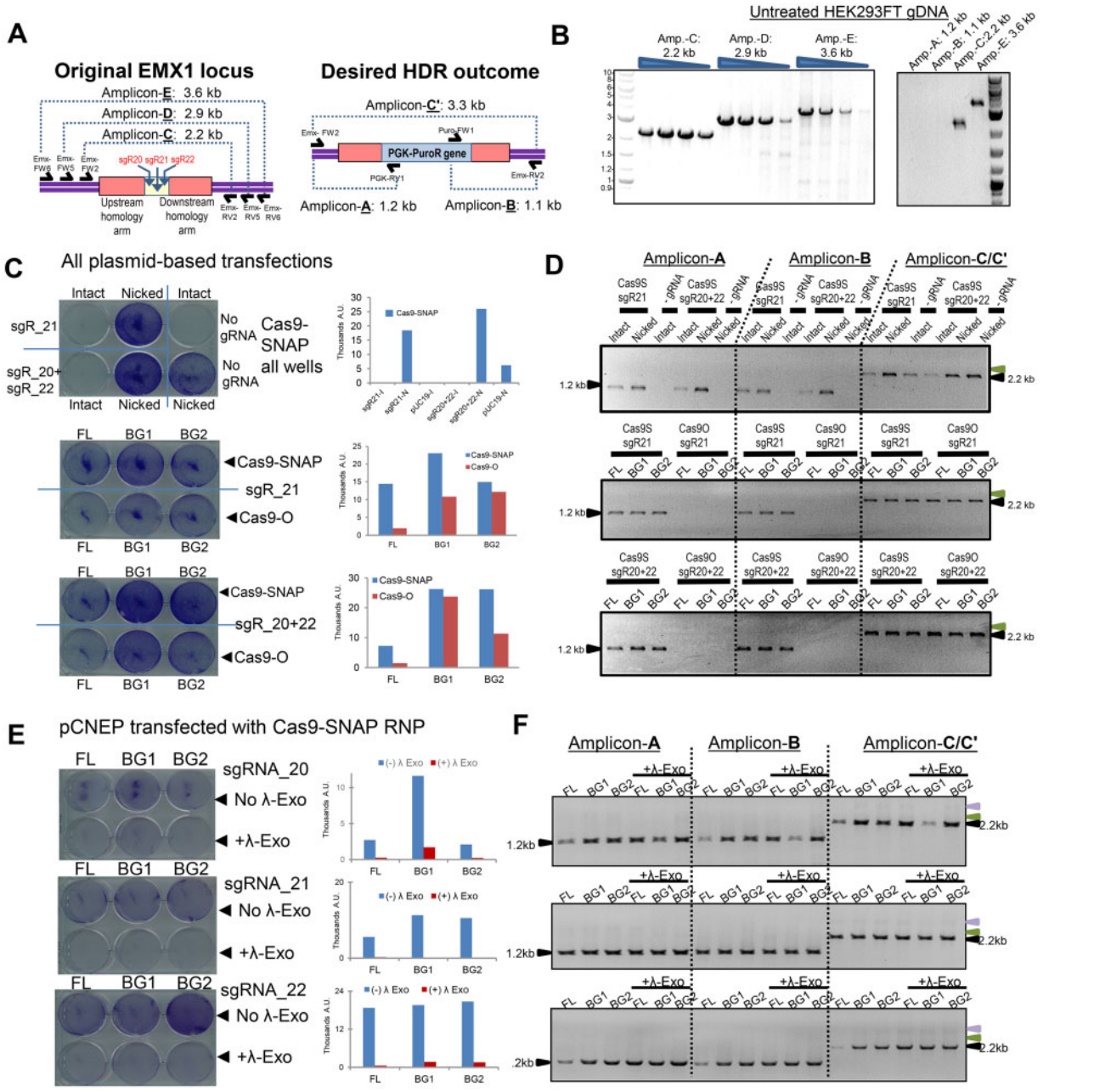

Figure 2 Measuring HDR at the *EMX1* locus from transfection of plasmids that can tether to Cas9-SNAP. (A) Schematic of genomic PCR to differentiate endogenous *EMX1* loci from desired HDR events. (B) PCR conditions amplify large amplicons from the *EMX1* locus (left), and no artifacts from primers specific for puromycin transgene HDR template with untreated cells (right). (C) Crystal violet staining of puromycin-selected cells transfected with plasmids expressing Cas9-SNAP *vs* Cas9-Original (Cas9-O). Quantitation of the staining intensity in graphs on right. Plasmid HDR templates modified with the addition of FL, or a single BG (BG1), or two BG (BG2) for tethering to Cas9-SNAP. (D) For each set of 6-well plates, the respective genomic PCR analysis of HDR events from Amplicon-A, -B, and -C. The black arrowheads point to the 1.2 kb size of Amplicon-A and -B and the 2.2 kb size of Amplicon-C from the endogenous *EMX1* locus. A desired HDR event generating a 3.3 kb Amplicon-C' is not observed (green arrowhead). (E) Crystal violet staining and quantitation of puromycin-selected cells that have been transfected with Cas9-SNAP RNPs and plasmid templates. A λ-exonuclease treatment was also applied to remove nicked and unligated pCNEP repair templates. Quantitation of the staining intensity is represented in graphs. (F) For each set of 6-well plates, the respective genomic PCR analysis of HDR events from Amplicon-A, -B, and -C/C'. The black arrowheads point to the 1.2 kb size of Amplicon-A and -B and the 2.2 kb size of Amplicon-C from the endogenous *EMX1* locus. A desired HDR event generating a 3.3 kb Amplicon-C' is not observed (green arrowhead), but a faint >5 kb band is discernable (purple arrowhead).

negative control, FL-labeled HDR plasmid, and subjected the cells to puromycin selection. We found that BG-labeled intact plasmids yielded puromycin-resistant cell colonies only when Cas9-SNAP and sgRNA were present (Figure 2, C and D, middle and bottom rows). Interestingly, however, we obtained a number of cell colonies with BG-labeled nicked plasmids even in the absence of sgRNA (Figure 2C, Supplementary Figure S3, A and B). We reasoned that these cell colonies resulted from the random, nonspecific integration of the nicked plasmid. To support this notion, we showed that the λ-exonuclease treatment of intact plasmids which cleared residual nicked plasmids left during the BG-linked oligonucleotide labeling greatly reduced promiscuous integration events (Supplementary Figure S3, C–E).

We then performed rigorous genomic PCR analyses of the surviving cells to detect integration of the transgene at the *EMX1* locus. This included the transgene-spanning genomic PCR assay along with the standard PCR assay for amplifying left and right junctions across multiple experiments testing Cas9-SNAP *vs* original Cas9, several sgRNAs targeting *EMX1*, and various transgenes cloned into intact plasmids, nicked plasmids, or plasmids labeled with the BG- and FL- oligonucleotides, respectively (Figure 2, C–F).

Our results from these experiments frequently detected both Amplicon-A and -B consistently, indicating apparent *EMX1*-locus specific HDR. However, two perplexing issues remained: the BG-labeled plasmids were not significantly better than the FL-labeled plasmids, and we only detected the 2.2 kb Amplicon-C from the original *EMX1* locus lacking the transgene, while the 3.3 kb desired integrated transgene Amplicon-C' was extremely faint (Figure 2, E and F). The pre-coupling of BG-labeled plasmids to recombinant Cas9-SNAP (Ribonucleoprotein) RNP complex prior to transfecting cells yielded similar results to the previous experiments transfecting just Cas9-SNAP plasmid (Figure 2, E and F, Supplementary Figure S3). Although the misleading left and right junction amplicons suggesting apparent HDR were clearly detected in these selected cells, the transgene-spanning amplicons to indicate bona fide HDR were still absent.

This conundrum of detecting left and right junction amplicons but absence of the transgene-spanning amplicon was reminiscent of an earlier report of Southern blots unable to confirm robust junction amplicons from a TALEN-stimulated HDR effort in zebrafish (Won and Dawid 2017). Our negative results are incongruent with another study that claimed the BG-coupled ssODNs and Cas9-SNAP increased HDR-based editing (Savic *et al.* 2018), which did not control for the inherently higher HDR efficiency of unmodified ssODNs. As for blunt DNA amplicons, we also observed poor recovery of selected cells with BG-tagged blunt DNA templates (Supplementary Figure S1F). Perhaps the previous studies that only conducted left and right junction PCR assays overestimated the fidelity and efficiency of Cas9-stimulated HDR (Aird *et al.* 2018; Savic *et al.* 2018).

Cas9-stimulated HDR with a plasmid template results in integration of the bacterial vector backbone

To explain the failure of the transgene-spanning genomic PCR to detect apparently bona fide HDR events, we postulated that puromycin selection recovers mixed populations of cells with a rare number of true Cas9-stimulated HDR events overshadowed by a background of other spurious integrations of the puromycin marker (Rouet *et al.* 1994; Jasin and Haber 2016). Furthermore, we hypothesized that the 5'-to-3' DNA resection of the Cas9 cut site may expose just a single homology arm to invade the plasmid repair template during HDR, but that this event is stochastic in the mixed population of selected cells (Figure 3A). Provided this hypothesis is correct, the DNA synthesis would begin at a single homology arm and extend beyond the transgene to incorporate the plasmid vector backbone before NHEJ "repairs" the genomic locus. This putative mechanism would be analogous to "Break-Induced Replication" (BIR-like) DNA repair, as previously described for plasmid transgenesis in budding yeast and mammalian cells (Roth *et al.* 1985; Kramer *et al.* 1994; Kraus *et al.* 2001; Jasin and Haber 2016). Such a mechanism would allow plasmid bacterial vector backbone sequences to integrate at the *EMX1* cut site, thus making the transgene-spanning Amplicon-C' too large to be efficiently amplified from a single step genomic PCR because even hyper-processive polymerases would stumble on a > 6.5 kb amplicon if just one plasmid backbone inserts at the *EMX1* locus, or an even longer amplicon if a plasmid concatemer had inserted (AmpC', Figure 3A).

To verify this hypothesis, we conducted genomic PCR from selected population of cells using one primer near the *EMX1* cut site and additional primers complementary to three sections across the bacterial plasmid backbone (Figure 3B). This resulted in amplification of several discrete PCR products, clearly indicating the integration of extended portions of plasmid backbone (Figure 3C). Cloning and sequencing of these amplicons confirmed the junction between the plasmid bacterial backbone and the *EMX1* locus (Figure 3D). Two notable findings of this analysis were: (1) the plasmid bacterial backbone integration extended further on the downstream side of the puromycin transgene compared to the upstream side (Figure 3B), and (2) Sanger sequencing showed that while the chromatogram peaks in the plasmid region were well-phased, they were muddled in the *EMX1* locus (Figure 3E). These results are consistent with HDR initiating at one homology arm and NHEJ introducing small mutations at the other repair junction of the integrated transgene that would affect the Sanger sequencing phasing.

We considered this hypothesis of one-sided strand invasion as a possible HDR mechanism that would accept repair templates comprised of lssDNAs or Mini-circle DNAs (MC-DNA). Unfortunately, we also found that lssDNAs and MC-DNA constructs against the *EMX1* locus also performed poorly for bona fide Cas9-stimulated HDR (see Supplemental Text and Supplementary Figure S4).

Most of the previous studies assumed that amplification of the left and right HDR junctions is reflective of efficient and accurate integration of a transgene, (Ran *et al.* 2013a; Lin *et al.* 2014; Byrne *et al.* 2015; Chu *et al.* 2015; Maruyama *et al.* 2015; Gutschner *et al.* 2016; He *et al.* 2016a), which our results clearly indicated is not the case (Figure 2). We found that in most instances, the HDR was initiated at a single homology arm, and as a result, the strand synthesis continued past the other arm, thereby incorporating the plasmid backbone sequences (Figure 3). This finding is consistent with recent reports indicating the Fanconi anemia DNA repair pathway as a cellular response after a Cas9-mediated double-stranded break (DSB) (Davis and Maizels 2014; Davis and Maizels 2016; Richardson *et al.* 2018). Our results regarding HDR of the plasmid template may be a mixture of single-stranded template repair via the Fanconi anemia pathway and BIR. Our findings also explain the conundrum of Southern blots unable to detect left- and right-junction-spanning PCR amplicons in zebrafish (Won and Dawid 2017) and in mice (Skryabin *et al.* 2020), because integration of plasmid vector sequences along with the repair template alters the genomic locus away from the desired seamless integration of the transgene.

Bona fide Cas9-stimulated HDR with long 3' single-stranded overhangs (L3SSO) and BL3SSO repair templates

At this juncture, we became inspired by the model of chromosomal capture of a targeting fragment (Jasin and Haber 2016), and hypothesized that a hybrid dsDNA with two single-stranded homology arms as 3' overhangs could be poised to base-pair with single-stranded ends exposed after 5'-to-3' DNA resection of the Cas9 cut site. To test this model, we generated an HDR template carrying a puromycin selection marker flanked on either side by approximately 100 bp homology arms, with each arm containing an opposite-facing nicking site (Supplementary Figure S5). We

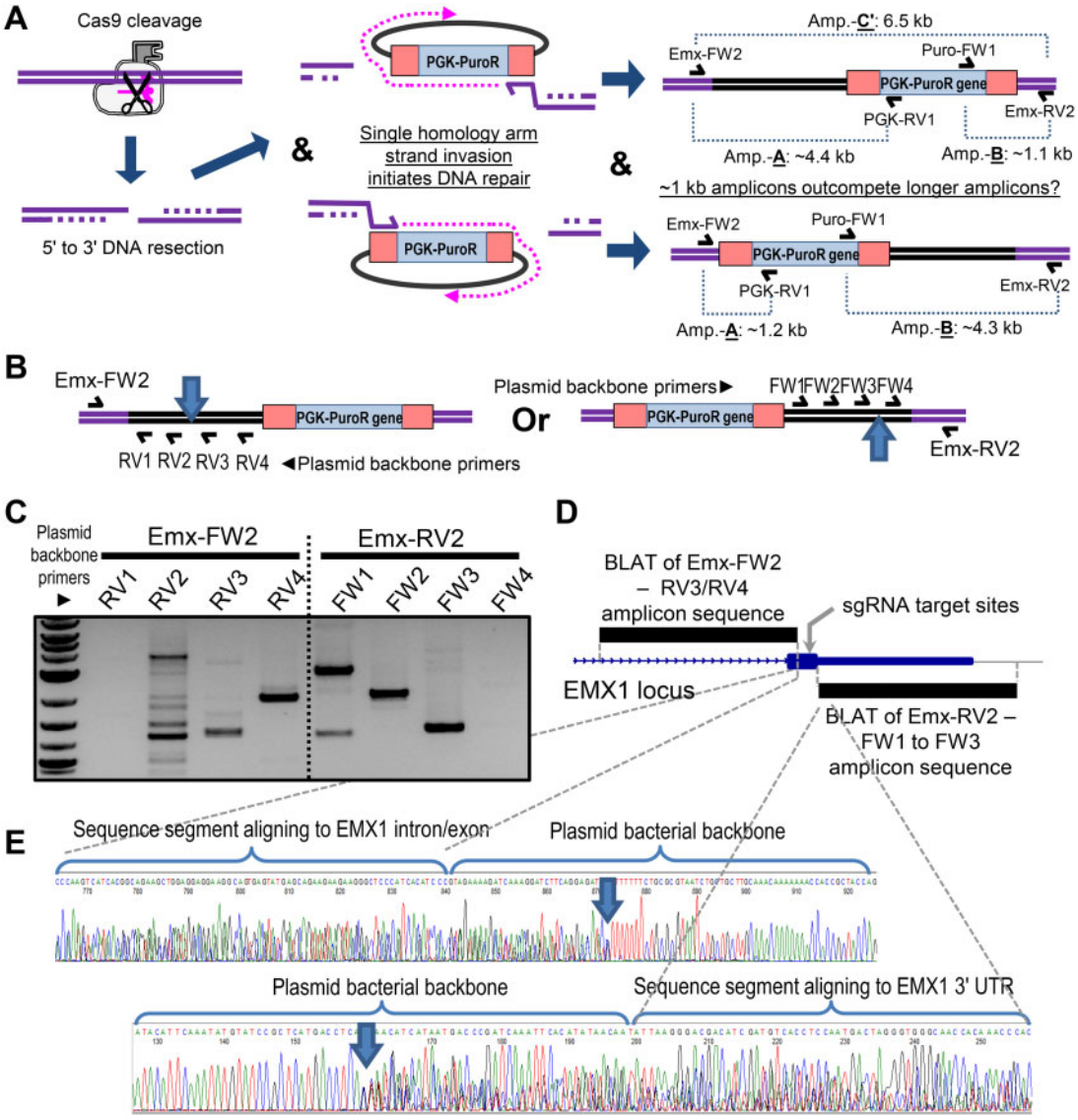

Figure 3 Plasmid bacterial sequence backbone integration during Cas9-stimulated HDR. (A) Hypothetical mechanism for plasmid backbone integration during Cas9-stimulated HDR. Mixed cell populations would contain both repair outcomes. (B) Design of PCR primers to detect plasmid backbone integration at the *EMX1* locus. (C) Genomic PCR amplicons from HEK293FT cells selected from Cas9-HDR of pCNEPm3 plasmid. (D) BLAT analysis maps amplicons to the *EMX1* locus, confirming HDR-mediated integration of plasmid backbone. (E) Sanger sequencing traces around the junction of plasmid backbone and *EMX1* integration site, showing the decrease in trace fidelity around repair junctions.

cloned this construct into a plasmid and subjected the resulting plasmid DNA to asymmetric nicking with the Nt.BbvCI endonuclease followed by DNA denaturation and gel purification. This yielded sufficient amounts of long 3' single-stranded overhang (L3SSO, pronounced like "lasso") repair template for transfection into cells (~15 μg L3SSO = ~15.5 pmoles).

To test the performance of L3SSO template when it was cloned into a plasmid *vs* when it was in the purified form, we transfected HEK293FT cells with either the plasmid carrying the L3SSO cassette or increasing amounts of the purified L3SSO DNA (0.2 and 1.0 μg), along with the Cas9-SNAP RNP. We then subjected these cells to puromycin selection and compared the number of recovered colonies between different conditions. Interestingly, while only a few colonies were seen for the plasmid-transfected cells, a large number of colonies were obtained for the cells transfected with 1.0 μg of the purified L3SSO template (Supplementary Figure S5B). PCR amplification of the transgene junction sites showed that both the plasmid and the purified L3SSO mediated the transgene integration, as observed with previous repair templates. However, a PCR spanning the whole transgene still suggested extremely poor integration efficiency (data not shown).

For highly sensitive detection of transgene integration, and to distinguish bona fide insertion of the full-length transgene from aberrant HDR events, we employed a Poison Primer Nested PCR approach (Edgley *et al.* 2002), which uses a poison primer to handicap the amplification of the unedited genomic locus (Supplementary Figure S5C; Amplicon-C_2, different label from Amplicon-C because this C_2 product is generated by the poison primer oligonucleotide set), thereby allowing preferential amplification of the locus modified by the transgene integration (Supplementary Figure S5C; Amplicon-C_2'). With this approach, we were finally able to detect the insertion of the full-length puromycin-resistance gene when 1.0 μg of L3SSO DNA was used (Supplementary Figure S5D; Amplicon-C_2'). Interestingly, higher integration efficiency was observed with sgRNA_21 as compared to the combination of sgRNA_20 and sgRNA_22. These results

could be replicated in independent L3SSO transfection experiments. Applying the Poison Primer Nested PCR approach to other tethered plasmids, lssDNAs, and MCs were still unable to amplify a transgene-spanning Amplicon-C_2' (data not shown).

Sequencing of multiple Amplicon-C_2' clones from L3SSO experiments confirmed the identity of full-length transgene integrated into the *EMX1* locus (Supplementary Figure S5E). However, two sets of clones revealed an asymmetric repair event: while the downstream L3SSO that included the Nt.BbvCI sites was correctly integrated at the Cas9 cut site, the upstream L3SSO was absent and repaired by gene conversion from the endogenous EMX1 locus. Furthermore, the PGK promoter was truncated to <50 and <13% of its original length in the two groups of clones.

Encouraged by the better performance of L3SSO templates, we further streamlined an entirely PCR-based procedure to generate BL3SSO templates with ~100 bp homology arms (Figure 4). This procedure relies on producing two PCR products, each containing a biotin moiety attached to one side of the amplicon. These PCR products are then captured on streptavidin beads, and the beads are subjected to denaturation to release the biotin-lacking strands followed by re-annealing of the retained strands. This is a fast procedure, allowing assembly of L3SSO templates within 48 hours. We were concerned that the biotin-conjugated L3SSO templates may still trigger DNA damage signaling upon transfection into cells (Shiotani and Zou 2009). We, therefore "blocked" each end of the template with the streptavidin protein (Figure 4A,

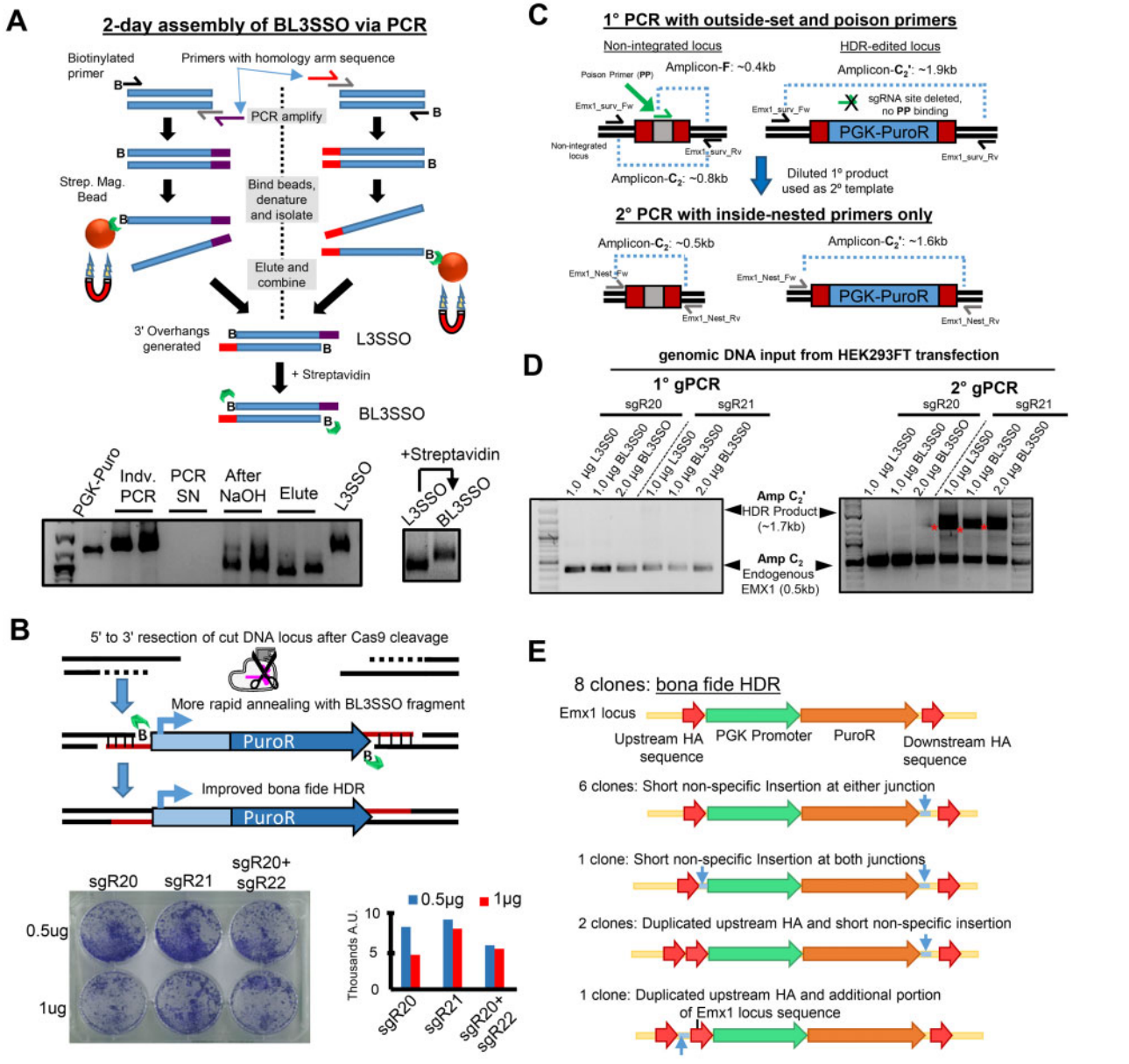

Figure 4 Cas9-stimulated HDR at *EMX1* with BL3SSO DNA template. (A) Schematic for generating L3SSO and BL3SSO DNAs from PCR-based approach. Gel image showing the PCR reaction, NaOH denaturing, strand separation, reformation of dsDNA (L3SSO), and addition of streptavidin protein (BL3SSO). (B) Model for improving bona fide HDR with representative experiment of Crystal Violet staining and quantitation of puromycin-selected HEK293FT cells transfected with Cas9-RNPs and BL3SSO template targeting *EMX1*. (C) Schematic of poison-primer approach to detect bona fide HDR insertions at the *EMX1* locus. (D) Representative genomic PCR analysis of the *EMX1* locus for integration of BL3SSO. Gel only shows 2° PCR products [C_2 and C_2', while 1° PCR gel (F, C_2, and C_2')] with poison primers not shown. (E) Diagrams of the sequenced clones from the Amplicon-C_2' products.

lower panel), which has been shown to mitigate DNA damage signaling in human cell extracts (Shiotani and Zou 2009). When transfected into HEK293FT cells along with the Cas9-SNAP RNP and appropriate sgRNA, the BL3SSO template gave rise to a large number of puromycin-resistant cell colonies (Figure 4B), which we then assayed by the transgene-spanning genomic PCR using poison primers (Figure 4C).

The PCR analysis showed that the BL3SSO template mediated robust HDR when used in combination with sgRNA_21, yielding strong DNA bands indicating integration of the full-length transgene for Amplicon-C_2' (Figure 4D). We subcloned this Amplicon-C_2' and analyzed it by DNA sequencing. Indeed, half of the 16 cell clones tested had bona fide, seamless integration of the HDR cassette with intact homology arms and PGK promoter, whereas the other half contained short nonspecific insertions or duplicated homology arms (Figure 4E). To quantitatively compare HDR efficiencies between the EMX1 L3SSO and BL3SSO *vs* plasmids templates, we deployed a droplet digital PCR (ddPCR) assay for measuring Cas9-stimulated HDR (Miyaoka *et al.* 2016), which provided absolute quantitation of proper transgene target insertions *vs* endogenous loci amplicons (Figure 5). We observed a ~5–7-fold improvement of HDR efficiency with EMX1 puromycin-resistance L3SSO and BL3SSO over plasmids (Figure 5, C and D), and reproducible HDR efficiency rates >10% with different EMX1-targeting sgRNAs (Figure 5, E and F). These results confirm that BL3SSO templates truly promote bona fide Cas9-stimulated HDR of long transgenes into an endogenous gene locus of a human cell line.

Leveraging BL3SSO to tag ISG loci

To demonstrate the utility of BL3SSO technology for inserting transgenes at other genomic loci, we pivoted our attention to interferon (IFN) ISGs, which are a cohort of genes stimulated in response to interferon treatment and virus infection (Noppert *et al.* 2007; Lukhele *et al.* 2019). Although there are exogenous transgene reporters with ISG promoters described in the literature (Pine *et al.* 1990; Patel *et al.* 2012; Gage *et al.* 2016; Vasou *et al.* 2018; Csumita *et al.* 2020), there is still an unmet need to generate mammalian cell lines with reporter genes inserted into endogenous ISG loci allowing for live tracking of antiviral immune responses to virus infection.

To address this need, we targeted two well-characterized ISGs, *Viperin*, also called *RSAD2* (Fitzgerald 2011), and *ISG15*. For *Viperin*,

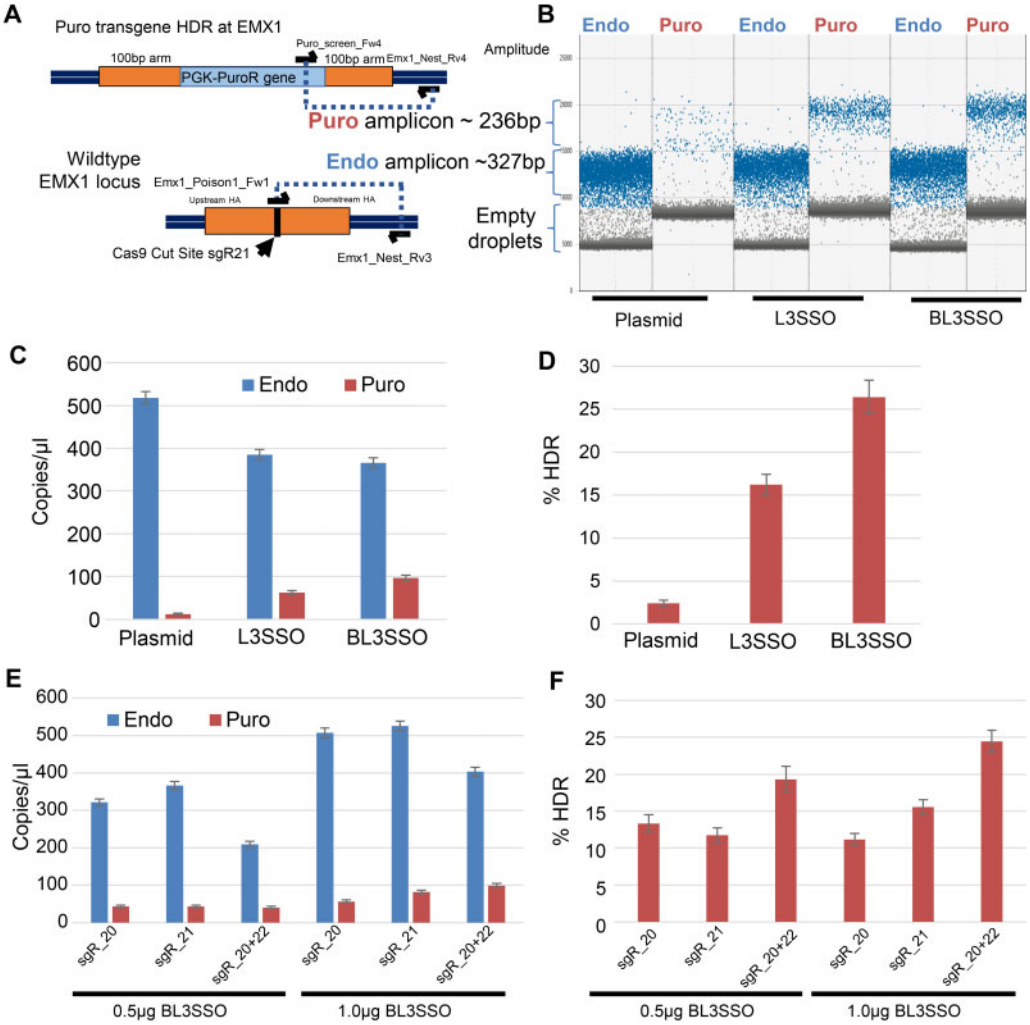

Figure 5 Droplet digital PCR (ddPCR) quantifies the improvement of Cas9-stimulated HDR with L3SSO and BL3SSO *vs* plasmid. (A) Schematic of primers and amplicons generated in the ddPCR assay against the *EMX1* locus. (B) Profiles of positive droplets (blue) over empty droplets (gray) enable direct quantitation of amplicons from HEK293 cells recovered from transgene and Cas9 transfection and puromycin selection. (C) Direct quantitation of molecules from the droplet profiles in (B,D) is the percent HDR calculated from (C) for the comparison of plasmid to L3SSO and BL3SSO targeted by sgRNA_21. Additional replicate experiments of just BL3SSO template in (E,F) testing different combinations of sgRNAs. All error bars represent the 95% confidence interval of the ddPCR quantitation algorithms based on the Poisson distribution.

we designed a BL3SSO template containing GFP and two homology arms; the right arm spanning the N-terminus of Viperin and the left arm covering the genomic region immediately upstream of the gene (Figure 6A). We then transfected this construct, along with Cas9 RNP and an sgRNA targeting the start codon of *Viperin* into HEK293T cells. Since Viperin is expressed in an IFN-dependent manner, we reasoned that its genomic locus may be silenced in the absence of interferon, thereby hindering the insertion of a heterologous sequence. Therefore, prior to transfection, we treated the cells with IFN-α for 24 hours. Flow cytometric analysis of the transfected cells showed that sgRNA2, one of the two Viperin sgRNAs tested, yielded relatively more GFP-positive cells (Figure 6, B and C), although the number of such cells was only less than 0.1%. Of note, BL3SSO templates performed marginally better than L3SSO templates (Figure 6D).

Next, we performed single-cell sorting of GFP-positive cells and isolated 22 individual clones. A single round of PCR showed that around 62% of these clones had GFP inserted into the *Viperin* locus (Figure 6E). As expected from the lower HDR efficiency, no homozygous-edited cells were obtained, and some clones displayed improper HDR with additional insertion of homology arms. We chose four of the PCR-validated cell clones for functional analyses and exposed them to two different concentrations of IFN-α for 48 hours followed by analysis of GFP expression by epifluorescence (Figure 6F). IFN treatment caused robust expression of GFP in two cell clones, #1A4 and #1C5, whereas the other two clones showed relatively lower expression. In contrast, no GFP positive cells were seen in the absence of IFN. Similarly, unedited HEK293FT cells did not fluoresce upon interferon treatment. To test if GFP was expressed as a fusion protein with Viperin, we performed Western blot analysis of all four clones using anti-Viperin and anti-GFP antibodies. Both unmodified and GFP-fused forms of Viperin were detected in all clones, confirming the previous observation that GFP was inserted into only one of the two alleles. Interestingly, the GFP-Viperin fusion protein accumulated to much higher levels than the unmodified protein, suggesting a stabilization effect of GFP on Viperin.

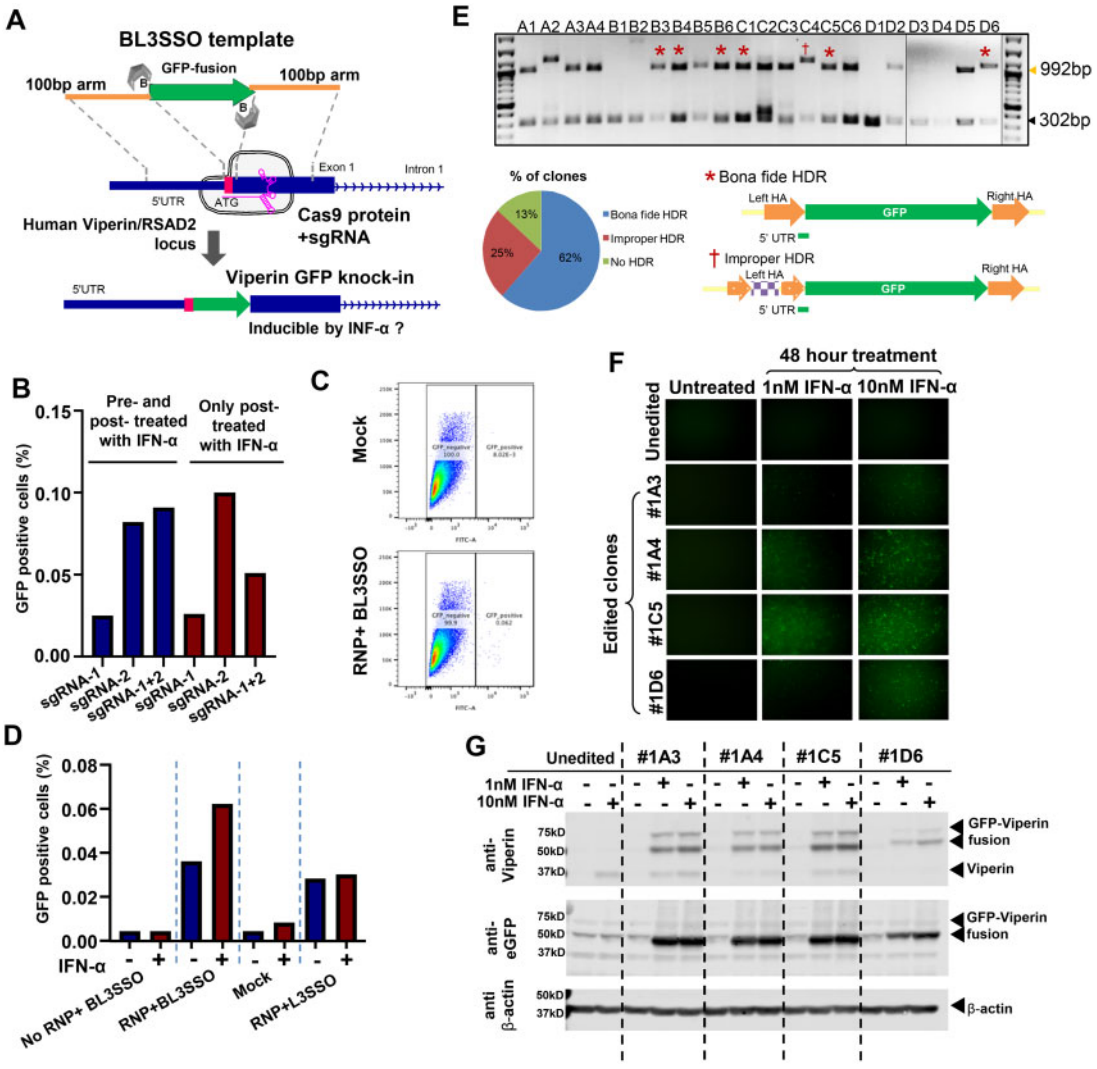

Figure 6 Cas9-mediated BL3SSO tagging of the endogenous human *Viperin/RSAD2* locus. (A) Schematic GFP BL3SSO template for N-terminus of human *Viperin* locus. (B) FACS analysis of GFP-positive HEK293FT cells after IFN-α treated at 48 hours after Cas9-sgRNA (Ribonucleoprotein-RNP) BL3SSO transfection. (C) FACS analysis of pre- and post- IFN-α treatment along with different sgRNAs. (D) Representative analytical FACS images show the percentage of GFP positive cells in a pool of HEK293FT cells. (E) Genomic PCR and Sanger sequencing of single FACS sorted GFP positive clones reveal mostly bona fide HDR and a few improper HDR outcomes. (F) GFP fluorescence of endogenously tagged *Viperin* locus in selected HDR positive clones at 1 and 10 nM IFNα treatment for 48 hours. (G) Western blot of endogenously tagged Viperin protein in HDR positive HEK293FT cell clones.

Next, we used BL3SSO to insert GFP into the endogenous locus of *ISG15* (Figure 7A). Similar to Viperin, less than 0.1% GFP-positive cells were recovered (Figure 7B); however, surprisingly, in contrast to Viperin-tagged cells, only two of the 16 single-cell clones tested (12.5%) showed bona fide HDR with GFP correctly inserted into the *ISG15* locus (Figure 7C). Other clones either lacked GFP insertion or showed DNA mutations at the junction site that would disrupt in-frame fusion between GFP and ISG15. We chose six PCR-validated cell clones for systematic analysis of GFP expression following IFN treatment. Interestingly, when

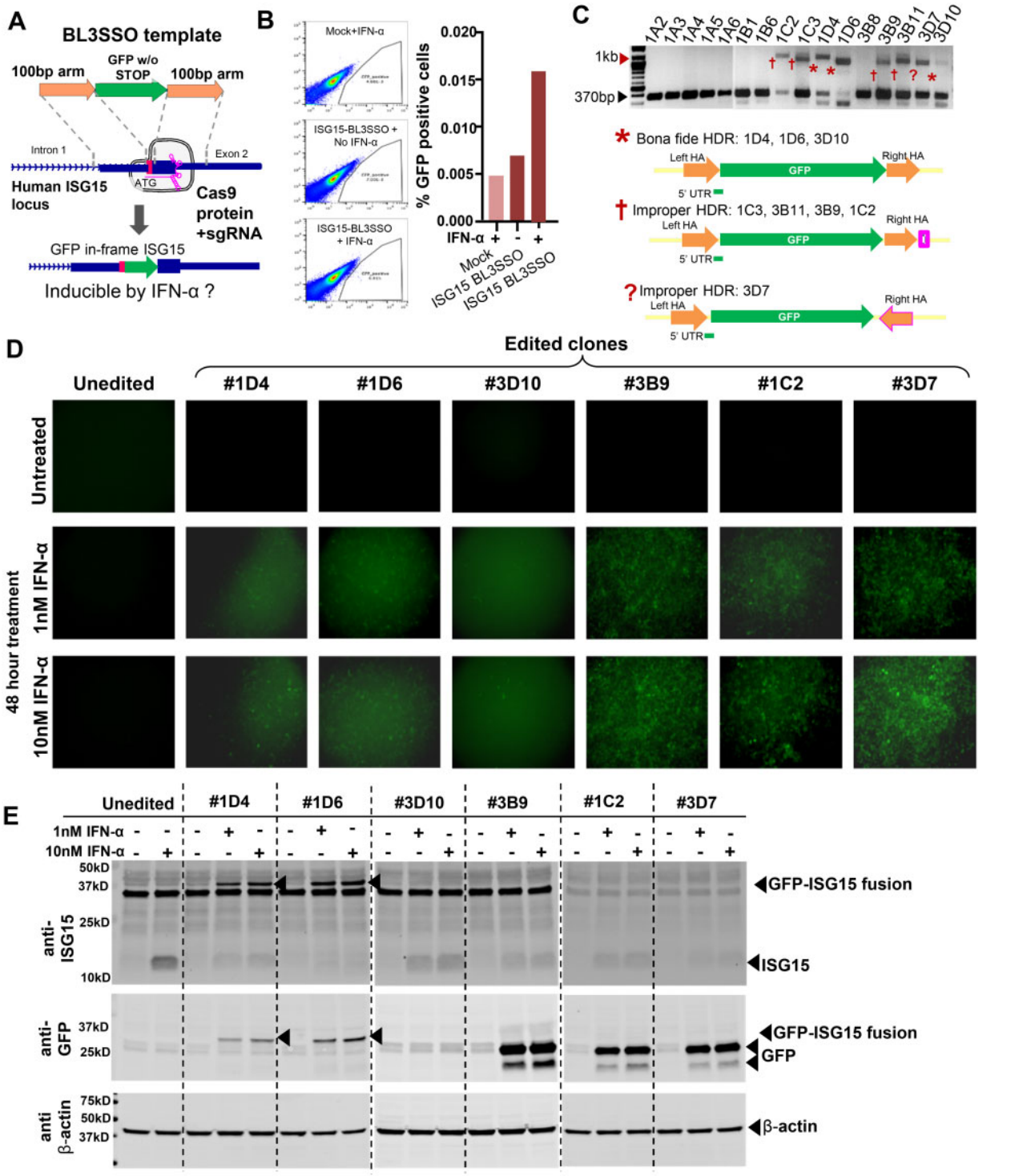

Figure 7 Cas9-mediated BL3SSO tagging of the endogenous human *ISG15* locus. (A) Schematic GFP BL3SSO template for N-terminus of the *ISG15* locus. (B) FACS analysis of GFP-positive HEK293FT cells after IFN-α treated at 48 hours after transfection of Cas9-sgRNA RNP and BL3SSO. (C) Genomic PCR and Sanger sequencing of single FACS sorted GFP positive clones reveal the variable outcomes of HDR tagging categorized as bona fide HDR and improper HDR. The small pink block represents various mutations that likely terminate translation downstream. (D) GFP fluorescence of endogenously tagged ISG15 locus in selected HDR positive clones at 1 and 10 nM IFN-α treatment for 24 and 48 hours. (E) Western blot of endogenously tagged ISG15 protein in HDR positive HEK293FT cell clones. Arrowheads point to the bands that are specifically recognized by the antibody. The offset of the GFP-ISG15 fusion arrowheads is because only clones #1D4 and #1D6 express the fusion.

tested by epifluorescence, all six clones expressed GFP in an IFN-dependent manner (Figure 7D), although much stronger GFP signal was obtained for clones with aberrant HDR, indicating higher accumulation and/or fluorescence of GFP when it is expressed in a nonfusion form. Western blot analysis confirmed these results, showing measurably higher abundance of GFP in clones where GFP was not fused with ISG15 (Figure 7E). Consistent with the PCR results, two clones, #1D4 and #1D6, expressed GFP-ISG15 fusion protein, as determined by immunostaining with anti-ISG15 and anti-GFP antibodies (Figure 7E). To explain why the cell clones with GFP insertions that are not perfectly fused to ISG15 appear brighter than the clones with perfect fusions to ISG15, the ubiquitin-like role of endogenous ISG15 (Ritchie and Zhang 2004) may likely impart more rapid turnover of GFP-ISG15 fusions than GFP by itself. In all, these data demonstrate that the BL3SSO system allowed successful insertion of a transgene into inducible genomic loci, such as those occupied by IFN-responsive genes.

Future optimization of BL3SSO templates to other cell types

Although the number of GFP-positive cells from ISG-targeting experiments was less than 0.1%, ISGs are expected to be one of the more challenging loci for HDR because IFN-induction has to open up the chromatin for Cas9 and BL3SSO templates to access. Other recent studies (He *et al.* 2016a, 2016b; Cai *et al.* 2019) measuring low efficiencies of Cas9-stimulated HDR of GFP transgene insertions in human cell lines including HEK293 cells are in accordance with our findings, yet contrast against other studies reporting higher efficiencies of GFP transgene insertions into safe-harbor loci like *ROSA26* and *AAVS1* (Ye *et al.* 2018; Jayavaradhan *et al.* 2019; Wierson *et al.* 2020; Yan *et al.* 2020), or in animals where embryonic cells are subjected to transgene and Cas9 injection (Paix *et al.* 2015; Dokshin *et al.* 2018; Gutierrez-Triana *et al.* 2018; Kina *et al.* 2019; Wierson *et al.* 2020), or treating cells with various cell-cycle drug inhibitors or adenoviral vectors (Lin *et al.* 2014; Gaj *et al.* 2017; Zhang *et al.* 2017). To our knowledge, no other study has examined Cas9-stimulated HDR targeting of ISG loci, so there is no directly relevant comparison to evaluate the rate of GFP-positive cells with BL3SSO targeting *Viperin* in HEK293 cells.

We are further optimizing the BL3SSO technology to overcome the challenges associated with the lower DNA transfection efficiency in some cell lines and variable knock-in efficiency at distinct genomic loci. For example, we failed to achieve HDR at the *EMX1* locus of RPE1, IMR-90, and BJ-Tert cells, which are considered more *in vivo*-like compared to HEK293FT cells but suffer from poor transfection efficiency (data not shown). Similarly, although we could successfully insert GFP at the *Piwi5* and *AGO3* loci in mosquito cells (Supplementary Figure S6, A and C), the GFP-positive cells failed to survive after bulk sorting. Likewise, despite initial evidence of a successful GFP integration at the *ISG56* and *AGO2* genes in HEK293FT cells (Supplementary Figure S6, B, D, and E), we could not recover the GFP-tagged cells nor could we insert GFP at the *ACE2* gene, the SARS-CoV-2 receptor and recently proposed to be an ISG (Ziegler *et al.* 2020). Nonetheless, these experiments provide a clear evidence that our BL3SSO technique is reproducible and superior to the plasmid-based HDR, since it obviates the integration of the plasmid backbone at the target site.

In summary, we have generated valuable HEK293FT cells with GFP insertions into *Viperin* and *ISG15*, providing the first reporter cell line permitting live tracking of bona fide cell-intrinsic responses to virus infection and interferon treatment. The impact on the biochemical functions of Viperin and ISG15 fused to GFP will be examined in future studies with these cells, such as more extensive examination of the kinetics of Type-I IFN induction responses, and potentially extending to SARS-CoV2 infections when these cells are further given ACE2-expressing transgenes. Perhaps post-translational regulation of Viperin and ISG15 may impact GFP expression and vice versa.

Acknowledgments

The authors are grateful to NEB staff members G. Brett Robb, Jennifer L. Cucuru, Megumu Mabuchi, and Ryan T. Fuchs for providing Cas9-SNAP protein and to Dianne Schwarz and Ezra Schildkraut for advice on the EnGen® sgRNA Synthesis kit and comments on the manuscript. They also thank Michael Blower, Rachel Flynn, and Daniel Cifuentes for comments on this manuscript.
J.A.K. and J.T. began the initial set of experiments, while S.B. and J.D. completed the remaining bulk of experiments. M.S. initiated collaboration to target ISG loci and provided significant guidance toward the project's completion. S.K., N.K., and F.F. assisted with western blots, J.B.C. and A.T. conducted final flow cytometry experiments, and N.C.L. also performed some experiments and wrote the study with input from all authors and members of the Lau lab. M.S. dedicates this manuscript to the memory of his late father, Muhammad Saeed Nasim, and N.C.L. dedicates it to the memory of his late mother, Margaret H.Y. Lau.

Funding

This work was supported by Brandeis University Sprout Grants, the Leir Foundation, a donation from M.H.Y. Lau, Boston University start-up funds, and the National Institutes of Health via R21HD088792, R01AG052465, and R01GM135215 to N.C.L. M.S. was supported by Boston University start-up funds.

Conflicts of interest

None declared.

Literature cited

Aird EJ, Lovendahl KN, St Martin A, Harris RS, Gordon WR. 2018. Increasing Cas9-mediated homology-directed repair efficiency through covalent tethering of DNA repair template. Commun Biol. 1:54.

Bottcher R, Hollmann M, Merk K, Nitschko V, Obermaier C, *et al.* 2014. Efficient chromosomal gene modification with CRISPR/cas9 and PCR-based homologous recombination donors in cultured Drosophila cells. Nucleic Acids Res. 42:e89.

Byrne SM, Ortiz L, Mali P, Aach J, Church GM. 2015. Multi-kilobase homozygous targeted gene replacement in human induced pluripotent stem cells. Nucleic Acids Res. 43:e21.

Cai Y, Cheng T, Yao Y, Li X, Ma Y, *et al.* 2019. In vivo genome editing rescues photoreceptor degeneration via a Cas9/RecA-mediated homology-directed repair pathway. Sci Adv. 5:eaav3335.

Chen B, Gilbert LA, Cimini BA, Schnitzbauer J, Zhang W, *et al.* 2013. Dynamic imaging of genomic loci in living human cells by an optimized CRISPR/Cas system. Cell. 155:1479–1491.

Chen F, Pruett-Miller SM, Huang Y, Gjoka M, Duda K, *et al.* 2011. High-frequency genome editing using ssDNA oligonucleotides with zinc-finger nucleases. Nat Methods. 8:753–755.

Chen JS, Dagdas YS, Kleinstiver BP, Welch MM, Sousa AA, *et al.* 2017. Enhanced proofreading governs CRISPR-Cas9 targeting accuracy. Nature. 550:407–410.

Chu VT, Weber T, Wefers B, Wurst W, Sander S, *et al.* 2015. Increasing the efficiency of homology-directed repair for CRISPR-Cas9-induced precise gene editing in mammalian cells. Nat Biotechnol. 33:543–548.

Codner GF, Mianne J, Caulder A, Loeffler J, Fell R, *et al.* 2018. Application of long single-stranded DNA donors in genome editing: generation and validation of mouse mutants. BMC Biol. 16: 70.

Cong L, Ran FA, Cox D, Lin S, Barretto R, *et al.* 2013. Multiplex genome engineering using CRISPR/Cas systems. Science. 339:819–823.

Csumita M, Csermely A, Horvath A, Nagy G, Monori F, *et al.* 2020. Specific enhancer selection by IRF3, IRF5 and IRF9 is determined by ISRE half-sites, 5' and 3' flanking bases, collaborating transcription factors and the chromatin environment in a combinatorial fashion. Nucleic Acids Res. 48:589–604.

Davis L, Maizels N. 2014. Homology-directed repair of DNA nicks via pathways distinct from canonical double-strand break repair. Proc Natl Acad Sci USA. 111:E924–E932.

Davis L, Maizels N. 2016. Two distinct pathways support gene correction by single-stranded donors at DNA nicks. Cell Rep. 17: 1872–1881.

Dokshin GA, Ghanta KS, Piscopo KM, Mello CC. 2018. Robust genome editing with short single-stranded and long, partially single-stranded DNA donors in *Caenorhabditis elegans*. Genetics. 210: 781–787.

Ebrahimi KH, Howie D, Rowbotham JS, McCullagh J, Armstrong FA, *et al.* 2020. Viperin, through its radical-SAM activity, depletes cellular nucleotide pools and interferes with mitochondrial metabolism to inhibit viral replication. FEBS Lett. 594:1624–1630.

Edgley M, D'Souza A, Moulder G, McKay S, Shen B, *et al.* 2002. Improved detection of small deletions in complex pools of DNA. Nucleic Acids Res. 30:e52.

Fitzgerald KA. 2011. The interferon inducible gene: viperin. J Interferon Cytokine Res. 31:131–135.

Fu Y, Yang Y, Zhang H, Farley G, Wang J, *et al.* 2018. The genome of the Hi5 germ cell line from Trichoplusia ni, an agricultural pest and novel model for small RNA biology. eLife. 7:e31628

Gage ZO, Vasou A, Gray DW, Randall RE, Adamson CS. 2016. Identification of novel inhibitors of the type I interferon induction pathway using cell-based high-throughput screening. J Biomol Screen. 21:978–988.

Gaj T, Staahl BT, Rodrigues GMC, Limsirichai P, Ekman FK, *et al.* 2017. Targeted gene knock-in by homology-directed genome editing using Cas9 ribonucleoprotein and AAV donor delivery. Nucleic Acids Res. 45:e98.

Gautier A, Juillerat A, Heinis C, Correa IR, Jr, Kindermann M, *et al.* 2008. An engineered protein tag for multiprotein labeling in living cells. Chem Biol. 15:128–136.

Gu B, Posfai E, Gertsenstein M, Rossant J. 2020. Efficient generation of large-fragment knock-in mouse models using 2-cell (2C)-Homologous Recombination (HR)-CRISPR. Curr Protoc Mouse Biol. 10:e67.

Gu B, Posfai E, Rossant J. 2018. Efficient generation of targeted large insertions by microinjection into two-cell-stage mouse embryos. Nat Biotechnol. 36:632–637.

Gutierrez-Triana JA, Tavhelidse T, Thumberger T, Thomas I, Wittbrodt B, *et al.* 2018. Efficient single-copy HDR by 5' modified long dsDNA donors. eLife. 7:e39468.

Gutschner T, Haemmerle M, Genovese G, Draetta GF, Chin L. 2016. Post-translational regulation of Cas9 during G1 enhances homology-directed repair. Cell Rep. 14:1555–1566.

He X, Tan C, Wang F, Wang Y, Zhou R, *et al.* 2016a. Knock-in of large reporter genes in human cells via CRISPR/Cas9-induced homology-dependent and independent DNA repair. Nucleic Acids Res. 44:e85.

He Z, Proudfoot C, Whitelaw CB, Lillico SG. 2016b. Comparison of CRISPR/Cas9 and TALENs on editing an integrated EGFP gene in the genome of HEK293FT cells. Springerplus. 5:814.

Hemmi H, Takeuchi O, Kawai T, Kaisho T, Sato S, *et al.* 2000. A Toll-like receptor recognizes bacterial DNA. Nature. 408:740–745.

Hwang WY, Fu Y, Reyon D, Maeder ML, Kaini P, *et al.* 2013a. Heritable and precise zebrafish genome editing using a CRISPR-Cas system. PLoS One. 8:e68708.

Hwang WY, Fu Y, Reyon D, Maeder ML, Tsai SQ, *et al.* 2013b. Efficient genome editing in zebrafish using a CRISPR-Cas system. Nat Biotechnol. 31:227–229.

Ishii KJ, Coban C, Kato H, Takahashi K, Torii Y, *et al.* 2006. A Toll-like receptor-independent antiviral response induced by double-stranded B-form DNA. Nat Immunol. 7:40–48.

Jasin M, Haber JE. 2016. The democratization of gene editing: insights from site-specific cleavage and double-strand break repair. DNA Repair (Amst). 44:6–16.

Jayavaradhan R, Pillis DM, Goodman M, Zhang F, Zhang Y, *et al.* 2019. CRISPR-Cas9 fusion to dominant-negative 53BP1 enhances HDR and inhibits NHEJ specifically at Cas9 target sites. Nat Commun. 10:2866.

Juillerat A, Gronemeyer T, Keppler A, Gendreizig S, Pick H, *et al.* 2003. Directed evolution of O6-alkylguanine-DNA alkyltransferase for efficient labeling of fusion proteins with small molecules *in vivo*. Chem Biol. 10:313–317.

Kim S, Kim D, Cho SW, Kim J, Kim JS. 2014. Highly efficient RNA-guided genome editing in human cells via delivery of purified Cas9 ribonucleoproteins. Genome Res. 24:1012–1019.

Kina H, Yoshitani T, Hanyu-Nakamura K, Nakamura A. 2019. Rapid and efficient generation of GFP-knocked-in Drosophila by the CRISPR-Cas9-mediated genome editing. Dev Growth Differ. 61: 265–275.

Komor AC, Badran AH, Liu DR. 2017. CRISPR-based technologies for the manipulation of Eukaryotic genomes. Cell. 168:20–36.

Kramer KM, Brock JA, Bloom K, Moore JK, Haber JE. 1994. Two different types of double-strand breaks in *Saccharomyces cerevisiae* are repaired by similar RAD52-independent, nonhomologous recombination events. Mol Cell Biol. 14:1293–1301.

Kraus E, Leung WY, Haber JE. 2001. Break-induced replication: a review and an example in budding yeast. Proc Natl Acad Sci USA. 98:8255–8262.

Lee SE, Moore JK, Holmes A, Umezu K, Kolodner RD, *et al.* 1998. Saccharomyces Ku70, mre11/rad50 and RPA proteins regulate adaptation to G2/M arrest after DNA damage. Cell. 94:399–409.

Lin S, Staahl BT, Alla RK, Doudna JA. 2014. Enhanced homology-directed human genome engineering by controlled timing of CRISPR/Cas9 delivery. eLife. 3:e04766.

Lindqvist R, Overby AK. 2018. The role of viperin in antiflavivirus responses. DNA Cell Biol. 37:725–730.

Lukhele S, Boukhaled GM, Brooks DG. 2019. Type I interferon signaling, regulation and gene stimulation in chronic virus infection. Semin Immunol. 43:101277.

MacDougall CA, Byun TS, Van C, Yee MC, Cimprich KA. 2007. The structural determinants of checkpoint activation. Genes Dev. 21: 898–903.

Mali P, Yang L, Esvelt KM, Aach J, Guell M, *et al.* 2013. RNA-guided human genome engineering via Cas9. Science. 339:823–826.

Maruyama T, Dougan SK, Truttmann MC, Bilate AM, Ingram JR, *et al.* 2015. Increasing the efficiency of precise genome editing with CRISPR-Cas9 by inhibition of nonhomologous end joining. Nat Biotechnol. 33:538–542.

Menendez-Arias L, Sebastian-Martin A, Alvarez M. 2017. Viral reverse transcriptases. Virus Res. 234:153–176.

Minev D, Guerra R, Kishi JY, Smith C, Krieg E, *et al.* 2019. Rapid in vitro production of single-stranded DNA. Nucleic Acids Res. 47: 11956–11962.

Miura H, Quadros RM, Gurumurthy CB, Ohtsuka M. 2018. Easi-CRISPR for creating knock-in and conditional knockout mouse models using long ssDNA donors. Nat Protoc. 13:195–215.

Miyaoka Y, Berman JR, Cooper SB, Mayerl SJ, Chan AH, *et al.* 2016. Systematic quantification of HDR and NHEJ reveals effects of locus, nuclease, and cell type on genome-editing. Sci Rep. 6:23549.

Noppert SJ, Fitzgerald KA, Hertzog PJ. 2007. The role of type I interferons in TLR responses. Immunol Cell Biol. 85:446–457.

Paix A, Folkmann A, Rasoloson D, Seydoux G. 2015. High efficiency, homology-directed genome editing in *Caenorhabditis elegans* using CRISPR-Cas9 Ribonucleoprotein complexes. Genetics. 201:47–54.

Paquet D, Kwart D, Chen A, Sproul A, Jacob S, *et al.* 2016. Efficient introduction of specific homozygous and heterozygous mutations using CRISPR/Cas9. Nature. 533:125–129.

Patel DA, Patel AC, Nolan WC, Zhang Y, Holtzman MJ. 2012. High throughput screening for small molecule enhancers of the interferon signaling pathway to drive next-generation antiviral drug discovery. PLoS One. 7:e36594.

Perng YC, Lenschow DJ. 2018. ISG15 in antiviral immunity and beyond. Nat Rev Microbiol. 16:423–439.

Pine R, Decker T, Kessler DS, Levy DE, Darnell JE. Jr., 1990. Purification and cloning of interferon-stimulated gene factor 2 (ISGF2): ISGF2 (IRF-1) can bind to the promoters of both beta interferon- and interferon-stimulated genes but is not a primary transcriptional activator of either. Mol Cell Biol. 10:2448–2457.

Quadros RM, Miura H, Harms DW, Akatsuka H, Sato T, *et al.* 2017. Easi-CRISPR: a robust method for one-step generation of mice carrying conditional and insertion alleles using long ssDNA donors and CRISPR ribonucleoproteins. Genome Biol. 18:92.

Ran FA, Hsu PD, Lin CY, Gootenberg JS, Konermann S, *et al.* 2013a. Double nicking by RNA-guided CRISPR Cas9 for enhanced genome editing specificity. Cell. 154:1380–1389.

Ran FA, Hsu PD, Wright J, Agarwala V, Scott DA, *et al.* 2013b. Genome engineering using the CRISPR-Cas9 system. Nat Protoc. 8: 2281–2308.

Richardson CD, Kazane KR, Feng SJ, Zelin E, Bray NL, *et al.* 2018. CRISPR-Cas9 genome editing in human cells occurs via the Fanconi anemia pathway. Nat Genet. 50:1132–1139.

Richardson CD, Ray GJ, Bray NL, Corn JE. 2016. Non-homologous DNA increases gene disruption efficiency by altering DNA repair outcomes. Nat Commun. 7:12463.

Ritchie KJ, Zhang DE. 2004. ISG15: the immunological kin of ubiquitin. Semin Cell Dev Biol. 15:237–246.

Roth DB, Porter TN, Wilson JH. 1985. Mechanisms of nonhomologous recombination in mammalian cells. Mol Cell Biol. 5:2599–2607.

Rouet P, Smih F, Jasin M. 1994. Expression of a site-specific endonuclease stimulates homologous recombination in mammalian cells. Proc Natl Acad Sci USA. 91:6064–6068.

Savic N, Ringnalda FC, Lindsay H, Berk C, Bargsten K, *et al.* 2018. Covalent linkage of the DNA repair template to the CRISPR-Cas9 nuclease enhances homology-directed repair. eLife. 7:

Shiotani B, Zou L. 2009. Single-stranded DNA orchestrates an ATM-to-ATR switch at DNA breaks. Mol Cell. 33:547–558.

Skryabin BV, Kummerfeld DM, Gubar L, Seeger B, Kaiser H, *et al.* 2020. Pervasive head-to-tail insertions of DNA templates mask desired CRISPR-Cas9-mediated genome editing events. Sci Adv. 6: eaax2941.

Vasou A, Paulus C, Narloch J, Gage ZO, Rameix-Welti MA, *et al.* 2018. Modular cell-based platform for high throughput identification of compounds that inhibit a viral interferon antagonist of choice. Antiviral Res. 150:79–92.

Veneziano R, Shepherd TR, Ratanalert S, Bellou L, Tao C, *et al.* 2018. *In vitro* synthesis of gene-length single-stranded DNA. Sci Rep. 8: 6548.

Wierson WA, Welker JM, Almeida MP, Mann CM, Webster DA, *et al.* 2020. Efficient targeted integration directed by short homology in zebrafish and mammalian cells. eLife. 9:e53968

Won M, Dawid IB. 2017. PCR artifact in testing for homologous recombination in genomic editing in zebrafish. PLoS One. 12: e0172802.

Yan N, Sun Y, Fang Y, Deng J, Mu L, *et al.* 2020. A universal surrogate reporter for efficient enrichment of CRISPR/Cas9-mediated homology-directed repair in mammalian cells. Mol Ther Nucleic Acids. 19:775–789.

Yao X, Zhang M, Wang X, Ying W, Hu X, *et al.* 2018. Tild-CRISPR allows for efficient and precise gene knockin in mouse and human cells. Dev Cell. 45:526–536.e525.

Ye L, Wang C, Hong L, Sun N, Chen D, *et al.* 2018. Programmable DNA repair with CRISPRa/i enhanced homology-directed repair efficiency with a single Cas9. Cell Discov. 4:46.

Zhang JP, Li XL, Li GH, Chen W, Arakaki C, *et al.* 2017. Efficient precise knockin with a double cut HDR donor after CRISPR/Cas9-mediated double-stranded DNA cleavage. Genome Biol. 18:35.

Ziegler CGK, Allon SJ, Nyquist SK, Mbano IM, Miao VN, HCA Lung Biological Network, *et al.* 2020. SARS-CoV-2 receptor ACE2 is an interferon-stimulated gene in human airway epithelial cells and is detected in specific cell subsets across tissues. Cell. 181: 1016–1035.e1019.

Communicating editor: J. K. Kim